# Quality Control of the Intrinsic Deposition Efficiency from the Controls of the Splat Morphologies and the Deposit Microstructure

*G. Montavon, C.C. Berndt, C. Coddet, S. Sampath, and H. Herman*

A simple heuristic model was developed to demonstrate the major characteristics of impinging particles prior to impact and during the spreading stages. It is based on the determination of transfer functions between the powder particle size distribution and splat equivalent diameter distributions. The input data consist mainly of the aforementioned distributions, determined experimentally using a particle size analyzer for powder particle size analysis and the wipe test for splat equivalent diameter analysis. Output data relate to the major characteristics of the impinging particles: flattening degree, intrinsic deposition efficiency, impact velocity, etc. Comparisons of the model predictions with experimental data showed reasonable agreement. Implementation of this simple protocol provides understanding of interactions during the process and also has technological and economical impacts. It permits quality control (QC) of deposition efficiency by control of splat morphologies and aids in the definition of specifications for the powders used (for example, in terms of the lower and upper limits of the particle size distribution leading to the formation of a deposit with given processing parameters) allowing the optimization of the spray parameters to obtain high-integrity deposits.

| Keywords | deposition efficiency, flattened particle, heuristic modeling, spray angle, spray parameters, vacuum plasma spraying |
|---|---|

## 1. Introduction

ALTHOUGH COMMONLY used in industry for many years, direct-current (DC) plasma spraying, especially in the form of vacuum plasma spraying (VPS), is still an empirical technology because of its complexity (more than 50 macroscopic parameters control the process). For example, the influence of coating microstructure on mechanical properties is not well understood. Other unknowns are the relationships between macroscopic spray parameters and coating microstructure. However, new applications, such as VPS forming of free-standing shapes, require better knowledge and control of coating formation.

Thermal spray technology, especially the use of plasma jets, is an innovative method in the materials processing field. The main advantages are versatility (spraying numerous materials: metallic alloys, ceramics, polymers, etc.) and the ability to build coatings on the surface of a great variety of substrates. Many applications include protection against corrosion oxidation, thermal barrier coatings (TBC); protection against wear, functional graded coatings (FGC); and free-standing forms with a range of thicknesses.

To obtain "good" quality deposits, all impinging particles, or at least the matrix of composite particles, deposited on the surface of the substrate (or on the top of the previously deposited

layers) must be melted or in a plastic state at the instant of impact. As a consequence, a major difficulty in the process is determining a trajectory and a suitable dwell time for particles in the plasma flame to transfer enough heat to allow melting of the feedstock materials and to achieve a velocity that permits formation of splatting on the surface to be coated.

This paper describes a simple heuristic model, which has been developed to approximate several known characteristic properties of the impinging particles leading to the formation of a thick deposit including flattening degree, impact velocity, and

G. Montavon and C. Coddet, Laboratoire d'Études et de Recherches sur les Materiaux et les Propriétés de Surface, Institut Polytechnique de Sevenans, BP 449, 90 010 Belfort Cedex, France; C.C. Berndt, S. Sampath, and H. Herman, The Thermal Spray Laboratory, Department of Materials Science and Engineering, State University of New York at Stony Brook, Stony Brook, NY 11794-2275, USA.

<table>
<tr><td colspan="2" align="center"><b>Nomenclature</b></td></tr>
<tr><td>$A$</td><td>splat area (mm$^2$)</td></tr>
<tr><td>$d$</td><td>powder particle diameter (mm)</td></tr>
<tr><td>$F(x)$</td><td>cumulative distribution of probability of powder particle sizes</td></tr>
<tr><td>$F(x')$</td><td>cumulative distribution of probability of splat equivalent diameters</td></tr>
<tr><td>$Re$</td><td>Reynolds number (dimensionless)</td></tr>
<tr><td>$T$</td><td>splat thickness (mm)</td></tr>
<tr><td>$v$</td><td>powder particle impact velocity (m · s$^{-1}$)</td></tr>
<tr><td>$V$</td><td>powder particle volume (mm$^3$)</td></tr>
<tr><td>$We$</td><td>Weber number (dimensionless)</td></tr>
<tr><td colspan="2" align="center"><b>Greek symbols</b></td></tr>
<tr><td>$\nu$</td><td>kinetic viscosity (m$^2$ · s$^{-1}$)</td></tr>
<tr><td>$\rho$</td><td>particle density (kg · m$^{-3}$)</td></tr>
<tr><td>$\sigma$</td><td>surface tension (N · m$^{-1}$)</td></tr>
<tr><td colspan="2" align="center"><b>Acronyms</b></td></tr>
<tr><td>DS</td><td>splat degree of splashing (dimensionless)</td></tr>
<tr><td>ED</td><td>splat equivalent diameter (mm)</td></tr>
<tr><td>EF</td><td>splat elongation factor (dimensionless)</td></tr>
</table>

intrinsic deposition efficiency. (A heuristic approach is different from an algorithm because it does not cover every possibility. It is not fully rational in the mathematical meaning of the term but
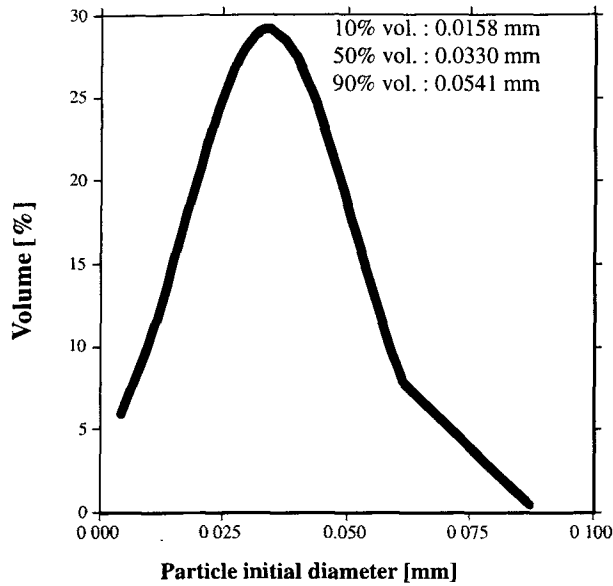


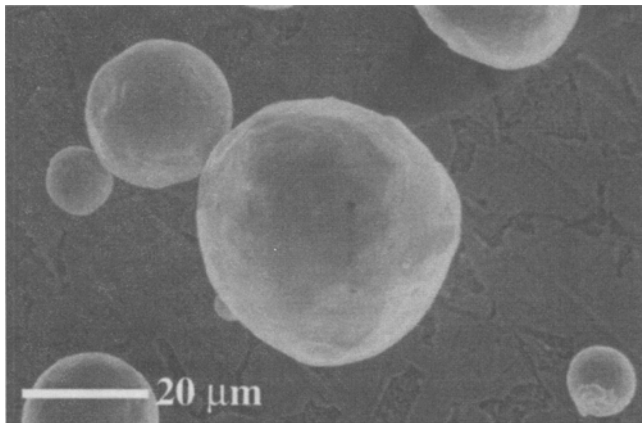**Fig. 1** Particle size distribution of the Astroloy powder



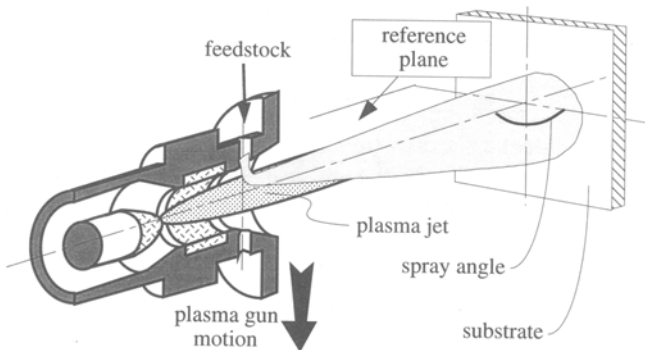**Fig. 2** Scanning electronic microscopy (SEM) view of the Astroloy powder



**Fig. 3** Schematic of the gun/substrate relative motion and definition of the spray angle

is capable of practical use in discovering a solution. An algorithm is a precise method of computation related to a model, that is, a step by step indication [Ref 1].) This model is driven by experimental data describing the morphology of splats collected on a polished substrate during the wipe test. In this work, Astroloy was sprayed on copper substrates using several processing parameters, such as spray parameters and spray angle. The model is compared with experimental data collected on thick deposits built with the same processing parameters.

## 2. Experimental Procedure and Preliminary Results

### 2.1 Experimental Procedure

#### 2.1.1 Material Characterization

The feedstock was a nickel-base alloy, known as Astroloy, of the chemical composition listed in Table 1, and of the particle size distribution, measured with a laser particle size analyzer, shown in Fig. 1. The particle morphology, illustrated in Fig. 2, is spherical. This shape is typical of a gas-atomized powder.

#### 2.1.2 Processing Parameters

Two sets of experiments were conducted. One set studied the effects of the spray parameters, and the other studied the effects of the spray angle. The flattened particle morphology study used

**Table 1** Chemical composition of Astroloy

| Element | Composition |
|---------|-------------|
| Nickel | Balance |
| Cobalt | 18.80 wt% |
| Chromium | 14.90 wt% |
| Molybdenum | 4.99 wt% |
| Aluminum | 3.99 wt% |
| Titanium | 3.55 wt% |
| Iron | 0.11 wt% |
| Zirconium | 0.04 wt% |
| Boron | 2,000 ppm |
| Carbon | 2,000 ppm |
| Silicon | 2,000 ppm |
| Oxygen | 85 ppm |
| Nitrogen | 29 ppm |
| Sulfur | 5 ppm |

**Table 2** Taguchi L8-$2^7$ alias structure

| Test | A | B | C | D | E | F | G |
|------|---|---|---|---|---|---|---|
| TA01 | - | - | - | - | - | - | - |
| TA02 | + | - | + | - | + | - | + |
| TA03 | - | + | + | - | - | + | + |
| TA04 | + | + | - | - | + | + | - |
| TA05 | - | - | - | + | + | + | + |
| TA06 | + | - | + | + | - | + | - |
| TA07 | - | + | + | + | + | - | - |
| TA08 | + | + | - | + | - | - | + |

The L8 designation refers to a two-level orthogonal matrix constituted by eight tests and extrapolated from a $2^7$ factorial design. The + and - signs represent upper and lower levels of design, respectively.

polished, pure copper substrates (ground with 600 grit SiC paper, followed by diamond slurry polishing using, in sequence, 5, 1, and 0.1 μm sized diamonds giving surface roughnesses, $R_a$, from 0.1 to 0.3 μm).

Thick deposits were sprayed using the same parameters. Here, the substrates were grit blasted (alumina particles of 300 μm average diameter), alcohol rinsed, and ultrasonically cleaned. After grit blasting, the substrate $R_a$ ranged from 2 to 3 μm.

The powder was vacuum plasma spray (VPS) processed in an inert residual atmosphere of argon, using a PT-VPS A-2000 system with a F4-VB torch (Sulzer-Metco AG, Rigackerstrasse 16, 5610 Wohlen, CH). In every case, the relative gun/substrate velocity was kept constant at 1 m · min⁻¹. The influences of the spray parameters were studied using Taguchi statistical experimental design. Design and the spray parameter sets, published in Ref 2 and 3, are summarized in Table 2 (Taguchi L8-2⁷ alias structure) and in Table 3 (spray parameters for VPS deposition). Five different spray angles were also tested to determine their influence at 90, 75, 60, 45, and 30 degrees. Spray angle was defined as the angle between the axis of the plasma gun and the surface of the substrate, in the plane orthogonal to the gun displacement, as illustrated in Fig. 3. Gun displacement was normal to the reference plane. Using this method, possible distortions of splats induced by the gun displacement did not interfere with those induced by the spray angle. For the spray angle testing, a "reference" spray parameter set was used, as listed in Table 4.

## Table 3  Spray parameters for VPS deposition

| Test | P1 | P2 | P3 | P4 | P5 | P6 | P7(a) |
|------|-----|-----|-----|-----|-----|-----|-------|
| TA01 | 650 | 60 | 60 | 6 | 300 | 4 | 20 |
| TA02 | 650 | 60 | 40 | 10 | 240 | 2.8 | 40 |
| TA03 | 650 | 120 | 60 | 6 | 300 | 2.8 | 40 |
| TA04 | 650 | 120 | 30 | 10 | 240 | 4 | 20 |
| TA05 | 720 | 60 | 60 | 6 | 240 | 2.8 | 40 |
| TA06 | 720 | 60 | 60 | 10 | 300 | 4 | 20 |
| TA07 | 720 | 120 | 40 | 6 | 240 | 4 | 20 |
| TA08 | 720 | 120 | 40 | 10 | 300 | 2.8 | 40 |
| TA09(b) | 700 | 60 | 50 | 8 | 270 | 3.4 | 30 |

P1, current intensity ($A$), P2, chamber pressure (mbar); P3, argon volume flow rate (1 · min⁻¹); P4, hydrogen volume flow rate (1 · min⁻¹); P5, spray distance (mm); P6, carrier gas (1 min⁻¹); P7, powder feed rate (g min⁻¹). (a) The powder feed rate was kept constant and equal to 3 g · min⁻¹ to collect individual splats onto the polished substrates. (b) Reference spray parameter set

## Table 4  Reference spray parameters for VPS deposition

| Parameter | Value |
|-----------|-------|
| Current intensity | 700 A |
| Chamber pressure | 60 mbar |
| Argon volume flow rate | 50 1 · min⁻¹ |
| Hydrogen volume flow rate | 8 1 · min⁻¹ |
| Spray distance | 270 mm |
| Carrier gas volume flow rate | 3.4 1 min⁻¹ |
| Powder feed rate | 30 g min⁻¹ |

Spray parameters developed at the LERMPS-IPSé

### 2.1.3  Particle Morphology Characterization

Splat characteristics were measured using the wipe test (Ref 4-6) and using optical microscopy and image analysis. Several size and shape factors were considered (Ref 2); (a) in particular, the equivalent diameter (ED), defined as the diameter of a circle with the same area as the selected feature; (b) the elongation factor (EF), defining the noncircular nature of the selected feature, unity being a perfect circle; and (c) the degree of splashing (DS), indicating the magnitude of peripheral material projections from the splats, generated on impact, and unity resulting from the absence of such projections. The mathematical relationships of these shape factors are as follows:

$$ED = \left( \frac{4 \cdot A}{\pi} \right)^{1/2} \tag{Eq 1}$$

$$EF = \frac{\pi}{4} \cdot \frac{L^2}{A} \tag{Eq 2}$$

$$DS = \frac{1}{4\pi} \cdot \frac{P^2}{A} \tag{Eq 3}$$

where $A$ is the area of the selected feature, $L$ is the longest dimension, and $P$ is the perimeter, as shown in Fig. 4. Due to mathematical definitions, there is a relationship between the elongation factor and the degree of splashing, as illustrated in Fig. 5. Hence, a "fictitious" degree of splashing is generated for high elongation factors. Under such conditions, raw data need to be corrected. Each measurement series of 50 readings was ran-
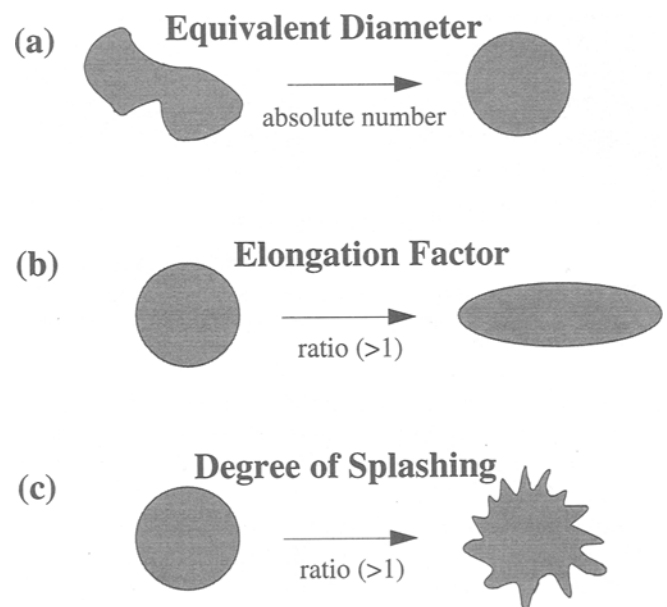


**Fig. 4**  Splat shape and size factors. The equivalent diameter is an absolute number, whereas the elongation factor and the degree of splashing are ratii greater than unity An increase of the elongation factor or the degree of splashing represents an increase in tendency to elongate or splash, respectively.
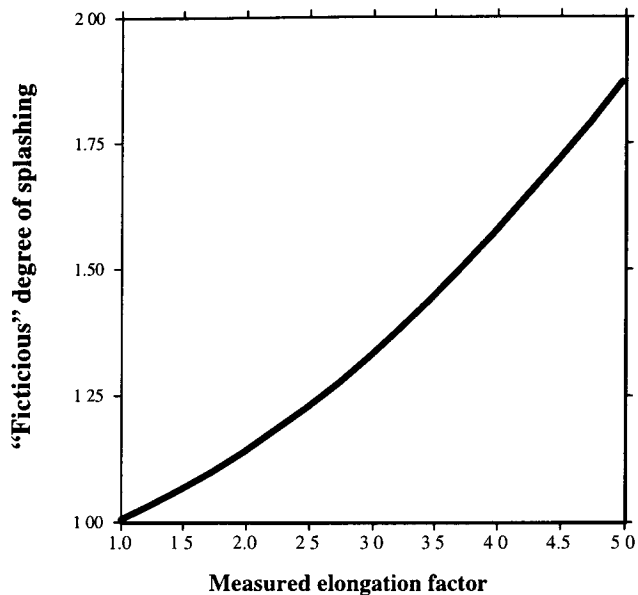
**Fig. 5** Evolution of the "fictitious" degree of splashing as a function of the elongation factor



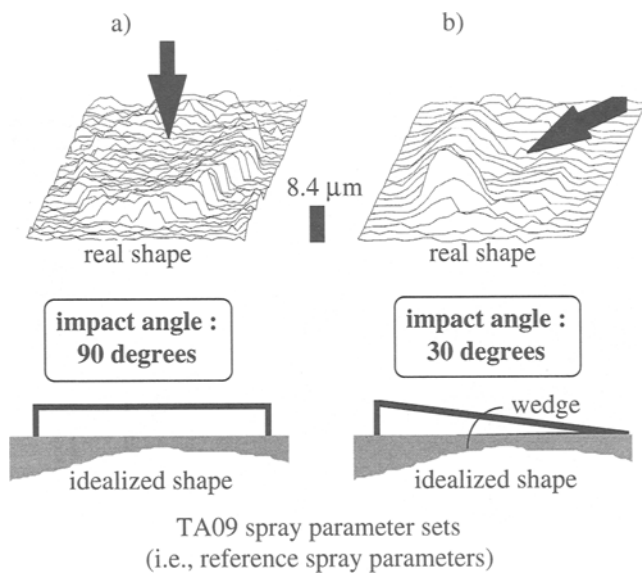**Fig. 6** Schematic of the scanning mechanical microscope (SMM)



**Fig. 7** Examples of typical measurements performed on splats with the SMM: (a) splat impacted with a normal angle and (b) splat impacted with an off-normal (30°) angle
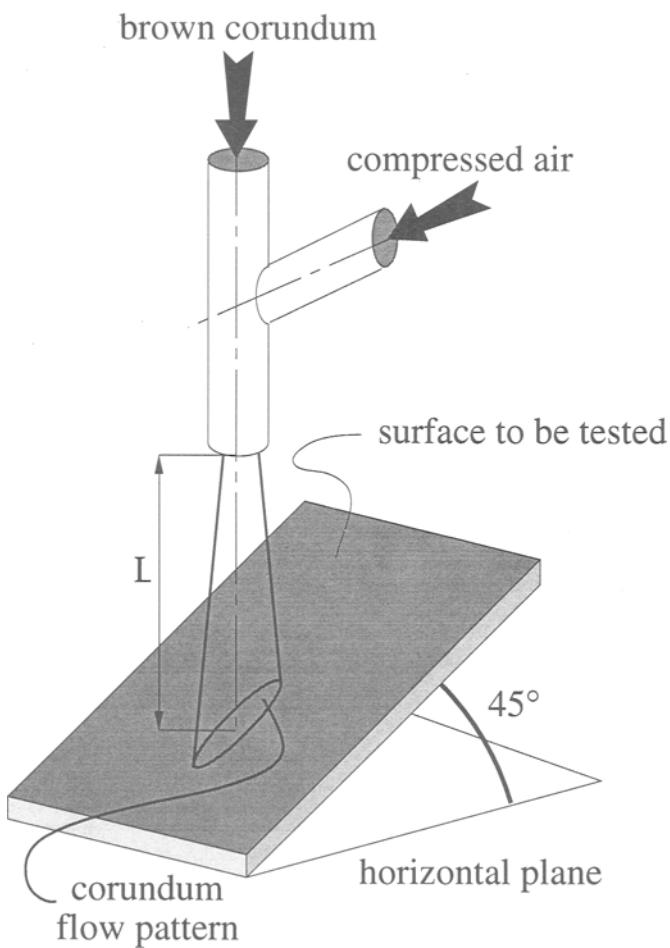


**Fig. 8** Schematic of the erosion wear resistance measurement facility

domly located along the specimens. Resulting data were adjusted by subtracting the two largest and smallest data points to discriminate against atypical values. Presented results refer to the adjusted data.

Some splat profiles were determined using a TRIDIM scanning mechanical microscope (SMM; Akilog, Chemin de l'Épitaphe, 25030 Besancon Cedex, France), illustrated in Fig. 6. A hemispheric diamond probe sensor, 1 μm in diameter, was used. Resolution of the apparatus was considered to be about 1 μm in the vertical direction and 2.5 μm in the horizontal direction (Ref 7). Contact force of the sensor was about 0.8 g, which was small enough not to pull splats out during the measurement. The ana-
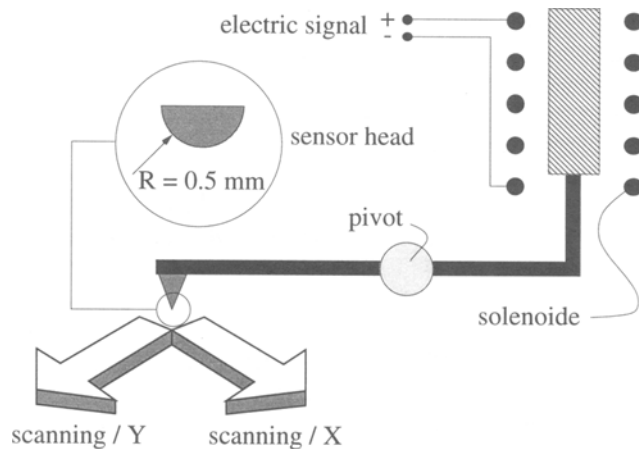
lyzed area (1.275 × 1.275 mm) was explored in increments of 5 μm. Due to the time needed to perform one measurement (a few hours), only two randomly chosen flattened particles were measured for each spray parameter set. Figure 7 displays examples of typical measurements. The peripheral splashes were not detected, indicating that their average thicknesses are lower than the SMM resolution in the vertical direction, 1 μm.

## Table 5 Processing parameters used to perform the erosion wear tests

| Parameter | Value |
|---|---|
| Particle nature | Calibrated brown corundum |
| Average diameter | 0 6 mm |
| Particle mass flow rate | $2 \, g \cdot min^{-1}$ |
| Air volume flow rate | $400 \, 1 \, min^{-1}$ |
| Impact angle | 45° |
| Nozzle/surface distance | 300 mm |
| Duration of the test | 10 min |

Angle between the centerline axis of the nozzle and the surface to be eroded

## Table 6 Deposit characteristics for different spray parameter sets

| Test | Porosity level, % | Erosion wear resistance, mg min⁻¹ | Deposition efficiency (1 = max) |
|---|---|---|---|
| TA01 | 1.15 (0 51) | (a) | 0.54 |
| TA02 | 1 13 (0.13) | 2.1 | 0.82 |
| TA03 | 0.70 (0.24) | (a) | 0.26 |
| TA04 | 0.74 (0.19) | 1.6 | 0.38 |
| TA05 | 1.49 (0.11) | 1.7 | 0.47 |
| TA06 | 1.11 (0.32) | 1.7 | 0.44 |
| TA07 | 0 40 (0.24) | 1.7 | 0.45 |
| TA08 | 0.70 (0 37) | 1.4 | 0.46 |
| TA09(b) | 1.31 (0.49) | 1.5 | 0.66 |

Average value and standard deviation (in parentheses) are obtained from ten measured fields (a) Unavailable data. (b) Reference spray parameter set

### 2.1.4 Deposit Microstructure Characterization

Thick sprayed deposits were cross-sectioned to make smaller coupons using a low-speed diamond saw in an oil medium. The coupons were degreased by immersion in alcohol and by placement in an ultrasonic cleaner. Next, they were mounted in epoxy rings, ground, and polished (grinding with 240 grit SiC paper followed by diamond slurry polishing using, in sequence, 45, 9, 3, and 1 μm sized diamonds). The deposit microstructures were characterized mainly by porosity level, which was determined using Delesse's principle (Ref 8) by image analysis (National Institutes of Health, Maryland, USA, software [Ref 9]). Resolution of this method is about 1 μm (Ref 10). Ten fields were measured on each specimen. The presented data refer to the average value and the standard deviation.

### 2.1.5 Erosion Wear Testings

Erosion wear resistance of the thick deposits was determined, not to measure resistance, but to characterize cohesion. A high erosion wear resistance always indicates a high level of cohesion of the deposit. Figure 8 describes the experimental device. A brown corundum grit flows through a nozzle and is accelerated by compressed air towards the surface to be eroded; it impacts on the surface at a 45° angle. Erosion wear resistance is then expressed as the weight loss per unit time (mg · min⁻¹) of the specimen. Table 5 summarizes processing parameters used for this work.
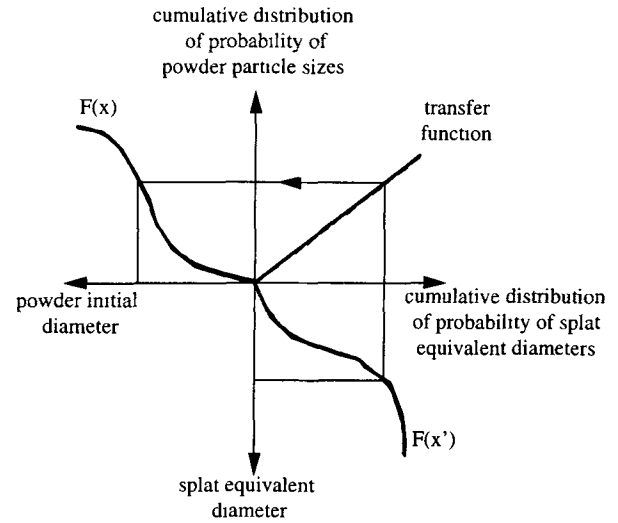


Fig. 9 Schematic of the heuristic model

### 2.2 Statistical Analysis

Gaussian analysis was used to assess the regularity of the data. The mean value (or expected value), $\mu$, and the standard deviation, $\sigma$, are used and defined as follows:

$$\mu = \sum_{all \, x} x \cdot f(x) \qquad (Eq \, 4)$$

$$\sigma = \left[ \sum_{all \, x} (x - \mu)^2 \, f(x) \right]^{1/2} \qquad (Eq \, 5)$$

where $f(x)$ is the probability density function of the distribution. The standard deviation is the measure of the absolute variation of data and depends on the scale of measurement All x signifies that the summation is done for "all x" (all valuesof the adjusted data) of the considered data.

### 2.3 Preliminary Results

#### 2.3.1 Effects of the Spray Parameters

Experimental effects of the spray parameters on the splat morphologies can be found in Ref 2 and 3. Table 6 lists the effects of these parameters on deposit characteristics (mainly porosity level), erosion wear resistance, and deposition efficiency.

Concerning erosion wear tests, weight loss of several Taguchi specimens is similar, with a 1.5 mg · min⁻¹ average value. Results indicate reasonable cohesion of the deposits, except for the TA02 deposit, which exhibits a significantly higher weight loss (2.1 mg · min⁻¹).

#### 2.3.2 Effects of the Spray Angle

Data relative to the effects of the spray angle on the splat morphologies can be found in Ref 3 and 11. Effects of the spray an-

gle on deposit characteristics (porosity level, erosion wear resistance, and deposition efficiency) are listed in Table 7.

Clearly, the spray angle significantly affects deposition efficiency; the lower the spray angle, the lower the deposition efficiency. The effect of spray angle on erosion wear resistance is also significant; the lower the spray angle, the higher the weight loss of the specimens and the lower the deposit cohesion.

## 3. Basis of the Heuristic Model

### 3.1 Heuristic Model

Cumulative probability distribution of splat equivalent diameters, $F(x')$, can be correlated with the cumulative probability distribution of the powder particle sizes, $F(x)$, through a theoretical transfer function, as illustrated in Fig. 9. The diameter of a powder particle, $d$, which could lead to formation of an observed splat of ED, can be calculated. Transfer functions need to be determined for the experimental sets. In this work, transfer functions were found to be similar because the equivalent diameter distributions were also similar; the spray parameter sets were close to the reference spray parameter set.

Knowledge of transfer functions, powder particle size distribution, and equivalent diameter distributions makes it possible

to analyze the deposit formation process, by iteration, as illustrated in Fig. 10.

Assuming that splats exhibit a constant thickness along a random cross section, and, conversely, have the same volume as initial powder particles, the theoretical splat thicknesses can be determined as follows:

$$T = \frac{V}{A} \tag{Eq 6}$$

where $V$ is the volume of an initial powder particle and $A$ is the area of the resulting splat.

The Yoshida (Ref 12), Trapaga (Ref 13), and Madejski (Ref 14) relationships establish, among others, a relationship between the dimensionless Reynolds number and the splat equivalent diameter on the powder particle initial diameter ratio. These relationships are expressed as follows:

$$\frac{ED}{d} = 0.89\,Re^{0.2} \text{ (Yoshida's relationship)} \tag{Eq 7}$$

$$\frac{ED}{d} = Re^{0.2} \text{ (Trapaga's relationship)} \tag{Eq 8}$$

$$\frac{ED}{d} = 1.29\,Re^{0.2} \text{ (Madejski's relationship)} \tag{Eq 9}$$

Knowledge of the Reynolds number of an impinging particle permits estimation of impact velocity if the kinetic viscosity of the molten material is known:

$$v = \frac{Re \cdot \nu}{d} \tag{Eq 10}$$

where $d$ is the powder particle initial diameter, $Re$ is the corresponding Reynolds number, and $\nu$ is the kinetic viscosity. Kinetic viscosity is critical in the experimental determination

**Table 7 Deposit characteristics for different spray angles**

| Spray angle, degrees | Porosity level, % | Erosion wear resistance, mg · min⁻¹ | Deposition efficiency (1 = max) |
|---|---|---|---|
| 90 | 1.31 (0.30) | 1.5 | 0.66 |
| 75 | 1.97 (0.30) | 1.6 | 0.35 |
| 60 | 2.63 (0.31) | (a) | 0.16 |
| 45 | 2.96 (0.60) | 1.9 | 0.11 |
| 30 | 3.08 (0.83) | 2.1 | 0 07 |

Average value and standard deviation (in parenthesis) obtained from ten measured fields. (a) Unavailable data

**Table 8 Comparison between calculated splat thickness values and experimental results**

| Test | Exp. ED(a), μm (±2.5 μm) | Exp. T(b), μm (±1 μm) | Cal. d(c), μm | Cal. T(d), μm | Difference, μm |
|---|---|---|---|---|---|
| TA01 | 115.5 | 3.9 | 39.0 | 3.0 | −0.9(f) |
| TA01 | 147.5 | 6.0 | 54.4 | 4.9 | −1.1 |
| TA02 | 85.0 | 2.2 | 30.5 | 2.6 | +0.4(f) |
| TA02 | 120.0 | 4.2 | 43.9 | 3.9 | +0.3(f) |
| TA03 | 85.0 | 2 0 | 30.5 | 2.6 | +0.6(f) |
| TA03 | 105.0 | 4.5 | 40.5 | 3.9 | −0.6(f) |
| TA04 | 95.0 | 3.1 | 32 4 | 2 5 | −0 6(f) |
| TA04 | 157 5 | 7.2 | 69.1 | 8.0 | +0.8(f) |
| TA05 | 52.5 | 1.5 | 14.2 | 0.7 | −0.6(f) |
| TA05 | 162.5 | 9.2 | 70.3 | 8.7 | −0.5(f) |
| TA06 | 60.0 | 2.1 | 20.1 | 1.5 | −0.6(f) |
| TA06 | 125.0 | 6.3 | 56.7 | 7.7 | +1.7 |
| TA07 | 67.5 | 2.4 | 26.6 | 2.7 | +0.3(f) |
| TA07 | 137.5 | 9.5 | 66.3 | 10.2 | +0.7(f) |
| TA09(e) | 97.5 | 3.5 | 38.8 | 4.1 | +0.6(f) |
| TA09(e) | 180.0 | 7.8 | 70.0 | 7.0 | −0.8(f) |

Note: The + signs refer to an overestimation of the calculation; the − signs refer to an underestimation of the calculation. (a) Exp. ED is experimentally measured splat equivalent diameter. (b) Exp. T is experimentally measured splat thickness. (c) Cal. d is calculated powder particle initial diameter. (d) Cal. T is calculated splat thickness. (e) Reference spray parameter set. (f) Difference lower than the spatial resolution of the scanning mechanical microscope

of this viscosity for molten Astroloy particles within a plasma plume, and because this value is not available in literature, the kinetic viscosity of pure nickel at the melting point (0.694 × 10⁻² m² · s⁻¹) (Ref 15) was used in the calculations because nickel is the primary element within Astroloy (67 wt.%).

The dimensionless Weber number establishes a relationship between the surface tension and the viscosity of a liquid (Ref 16), as follows:

$$We = \frac{d \cdot v^2 \cdot \rho}{\sigma} \tag{Eq 11}$$

where $d$ is the powder particle initial diameter, $\rho$ represents the density of the material at the temperature considered, and $\sigma$ is its surface tension. Again, the characteristic values of pure nickel at the melting point were used in the calculations (Ref 15), namely 1.778 N · m⁻¹ for the surface tension and 7905 kg · m⁻³ for the density.

## 3.2 Assumptions

The heuristic model is based on the following assumptions. The initial powder particle volumes are known and can be determined in this specific case because the initial powder particles exhibit near-spherical shapes.

There is no significant vaporization of powder particles during flight within plasma plume, that is, the mass conservation principle between the initial powder particle and the resulting splat.

At low pressure, when the ratio of the atomic/molecular mean free path to the particle diameter becomes higher than 0.01, the Knudsen effect, or "rarefaction" effect, may significantly reduce both heat flux from the plasma plume to small particles and the drag coefficient (Ref 17). Hence, the Knudsen
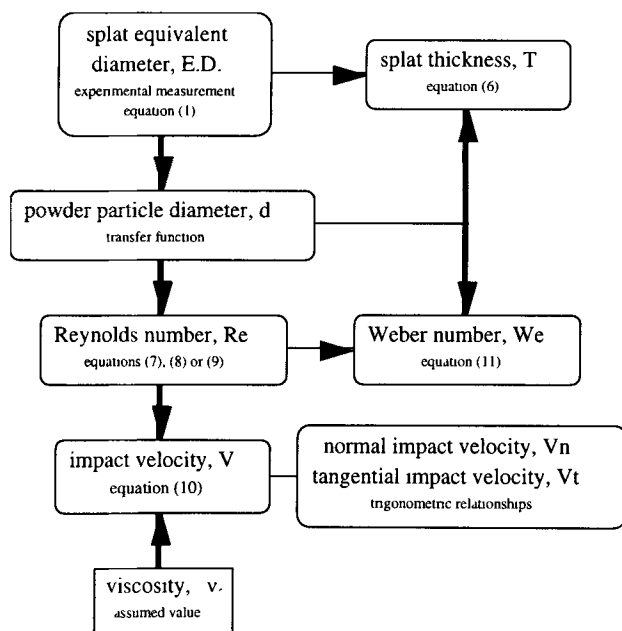
effect increases with decreasing particle size (Ref 18), and with increasing surface temperature of the particles (Ref 19). In thermal plasmas, this effect is emphasized for particle diameters less than 10 μm (Ref 17 to 19). This phenomenon was not taken into account because of the particle size distribution of the Astroloy powder; less than 2.5 vol% of particles have diameters smaller than 10 μm.

The splats exhibit near-perfect disc shapes (that is, constant thickness along a random cross section), with the thickness being small compared to the diameter (the experimental three-di-
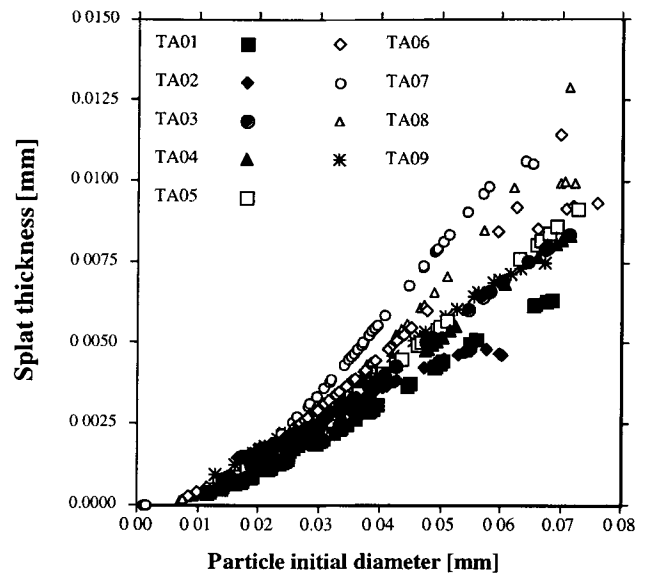


Fig. 11 Evolution of the splat thickness, $T$, as a function of the initial powder particle diameter, $d$, for several Taguchi spray parameter sets (TA01 to TA09)



Fig. 10 Major characteristics of powder particle, calculated by implementing the heuristic model
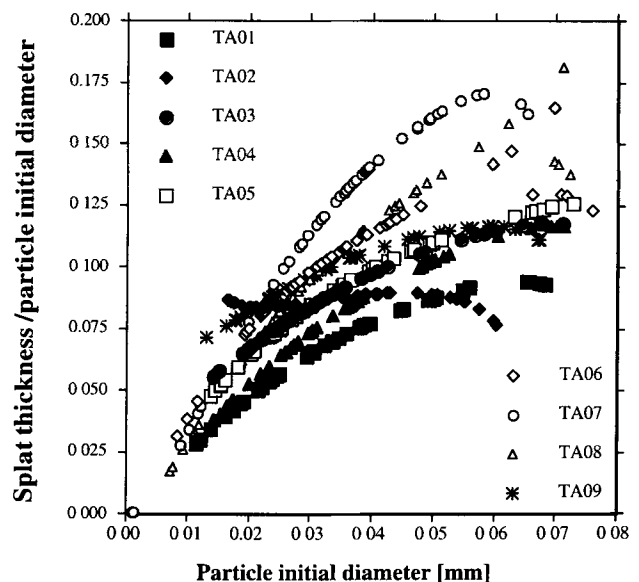


Fig. 12 Dependence of the ratio $(T/d)$ of splat thickness to initial powder particle diameter on the initial powder particle diameter $(d)$ for Taguchi spray parameter sets TA01 to TA09

mensional measurements performed over splats obtained with a 90° spray angle validate this assumption).

Powder particles of the same diameter show the same behavior within the plasma plume (that is, the same dwelling time, trajectory, thermal history, and velocity on impact).

# 4. Results and Discussion

## 4.1 Model Validation

Splat thicknesses (average values) were calculated using Eq 6, from determination of the equivalent diameter distributions and the transfer functions. Figure 11 shows the evolution of the splat thicknesses as a function of the calculated initial powder particle diameter for the various spray parameter sets (TA01 to TA09). The calculation shows that the splat thickness varies from approximately 1 μm to 12.5 μm. Spray parameters seem to have no significant effect on the resulting thickness of the smallest splats, indicating that impact velocities are probably identical. Figure 12 illustrates the dependence of the ratio of splat thickness to the initial powder particle diameter ($T/d$ ratio) on the initial powder particle diameter. Splat thickness is 6 to 40 times lower than the diameter of its original powder particle. The higher the $T/d$ ratio (the larger the initial powder particle), the less is the flattening of the splat. Splats sprayed with the TA02 spray parameter set are similar. The impinging particle diameter does not have a significant effect (in the considered range of diameters) on the resulting thickness of the splats; the $T/d$ ratio remains quasi-constant, equal to 0.08.

This heuristic model can be validated, at this stage of analysis, by comparison of the average thickness of the splats with experimental measurements, as illustrated in Table 8. The

calculated results agree with experimental measurements, the difference being generally lower than the spatial resolution of the SMM, except for two values (-1.1 μm for a TA01 measurement and +1.7 μm for another TA06 measurement). The initial assumption of mass conservation between the initial powder particle and the resulting splat seems valid under such conditions.

## 4.2 Deposition Efficiency

In thermal spraying, the intrinsic deposition efficiency is never equal to one. The intrinsic deposition efficiency is the highest efficiency that can be reached for a given feedstock and processing parameters. It does not consider substrate morphology or gun motion; it differs from the apparent deposition efficiency on actual shapes, known as target efficiency. A fraction of the injected feedstock does not become part of the deposit. It is interesting to calculate, a posteriori, the size distribution of the powder particles that lead to the formation of the collected splats by means of the transfer functions. Calculated secondary particle size distributions can be compared with the initial particle size distribution, determined experimentally (in this work, the size range is 5 to 88 μm, and the average diameter is 37 μm).

For each spray parameter set (TA01 to TA09), the calculated secondary particle size distributions, as well as the initial particle size distribution, are presented in Fig. 13. Spray parameters have a noticeable effect on the fraction of the particle size distribution effectively used to form splats; Fig. 14 details the lower and upper values of the secondary particle size distributions for each spray parameter set. Calculated average diameters of the secondary particle size distributions remain constant, equal to 35 μm. Such a value is very close to the measured average diameter of the actual particle size distribution (37 μm). It is likely
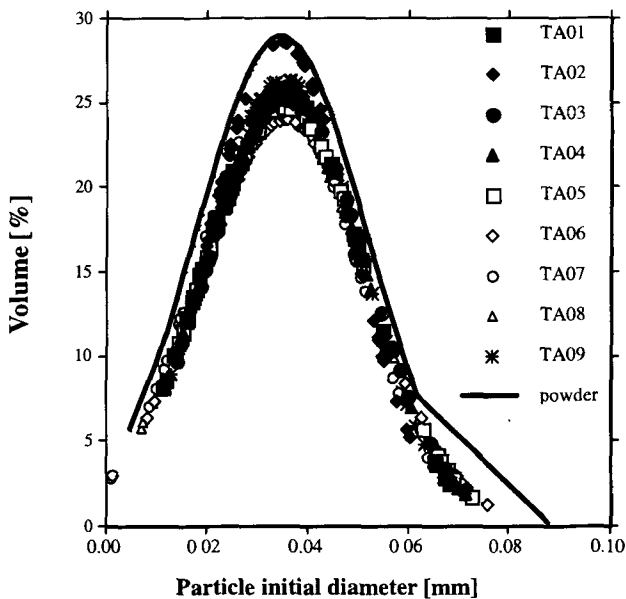


Fig. 13   Normal probability distributions of the initial powder particle diameters calculated using transfer functions, compared to the initial powder particle size distribution, for Taguchi spray parameter sets TA01 to TA09
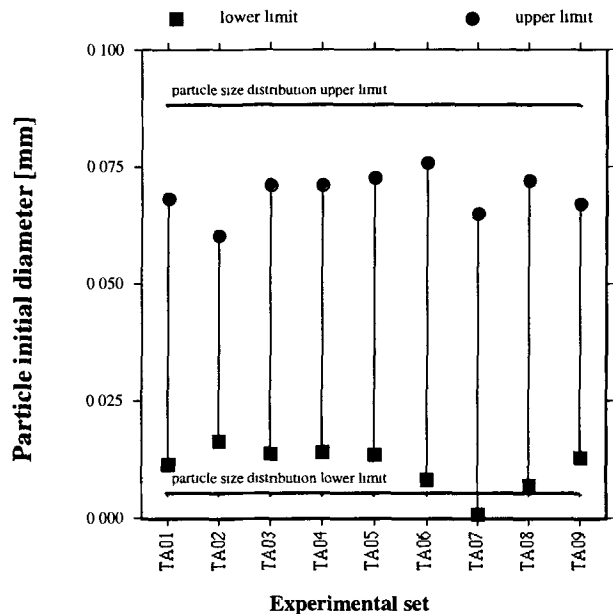


Fig. 14   Lower and upper limits of normal probability distributions of the initial powder particle diameters compared to the lower and upper limits of the initial powder particle size distribution for Taguchi spray parameter sets TA01 to TA09

that the smallest powder particles (diameter less than 15 μm) are vaporized within the plasma plume during flight, and that the biggest particles impact on the substrate either in a partially or fully unmolten state and rebound from the surface or strike with an impact velocity lower than the critical velocity necessary to induce spreading. This last phenomena is particularly empha-
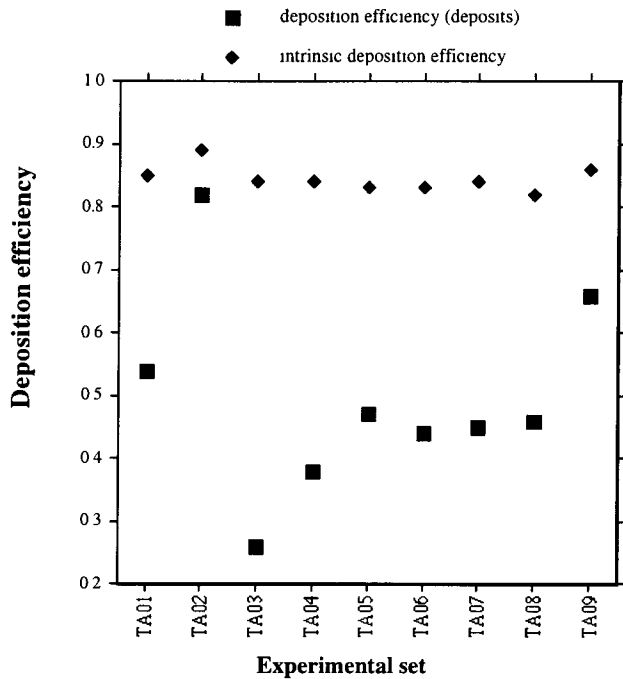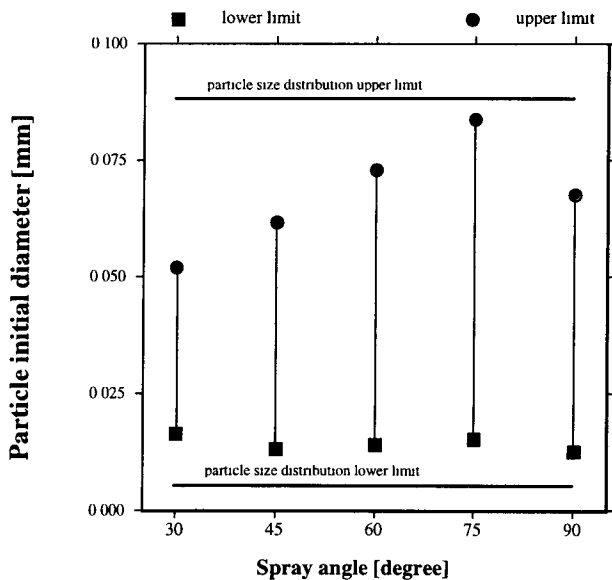
sized in the TA02 spray parameter set, which generates low-enthalpy plasma with low velocity. Figure 15 compares, for each spray parameter set (TA01 to TA09), the intrinsic deposition efficiencies, determined either experimentally from the characteristics of the deposits (measured deposition efficiency) or calculated from the secondary particle size distribution by summation (calculated deposition efficiency).

The two sets of results are similar qualitatively, except for those of the TA03 spray parameter set. Quantitatively, the measured deposition efficiencies are usually lower than the calculated efficiencies. The effect is induced by modifications of the
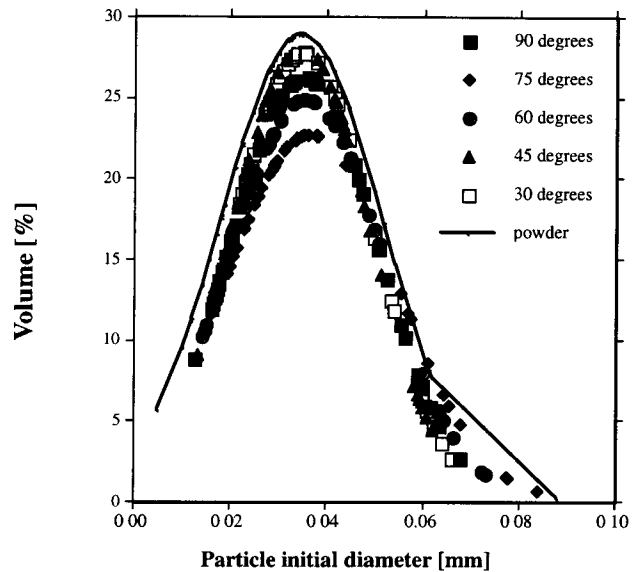


**Fig. 15** Comparison of the deposition efficiency measured on thick deposits, with the intrinsic deposition efficiency measured on splats, for spray parameter sets TA01 to TA09



**Fig. 16** Normal probability distributions of the initial powder particle diameters calculated using transfer functions, compared to the initial powder particle size distribution, for several spray angles (90° to 30°)
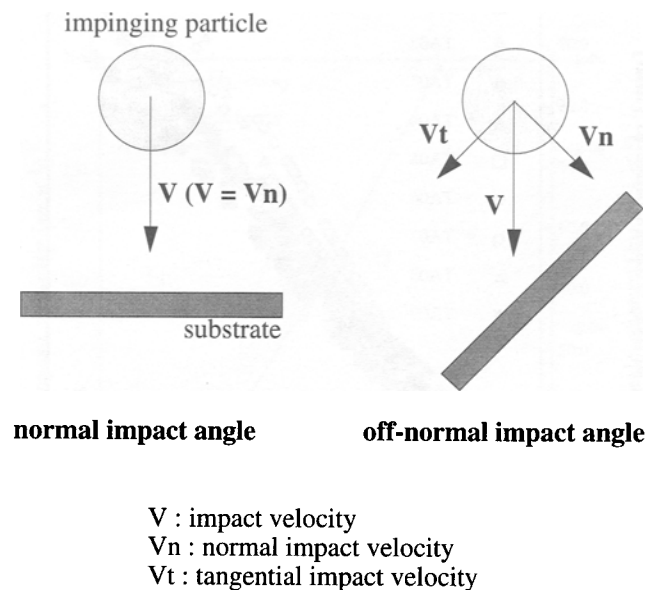


**Fig. 17** Lower and upper limits of normal probability distributions of the initial powder particle diameters, compared to the lower and upper limits of the initial powder particle size distribution, for several spray angles (90° to 30°)



**normal impact angle**          **off-normal impact angle**

V : impact velocity
Vn : normal impact velocity
Vt : tangential impact velocity

**Fig. 18** Schematic of the evolution of the impact normal and tangential velocities as a function of the spray angle

physical and chemical surface properties during formation of the thick deposits. The first layer is deposited onto the copper substrate, but subsequent layers are deposited onto the coating itself, which has different surface properties. The substrate temperature, higher in the case of thick deposits (±600 °C measured average value against 20 °C estimated value for the wipe test), can also substantially modify surface properties (Ref 20 and 21).
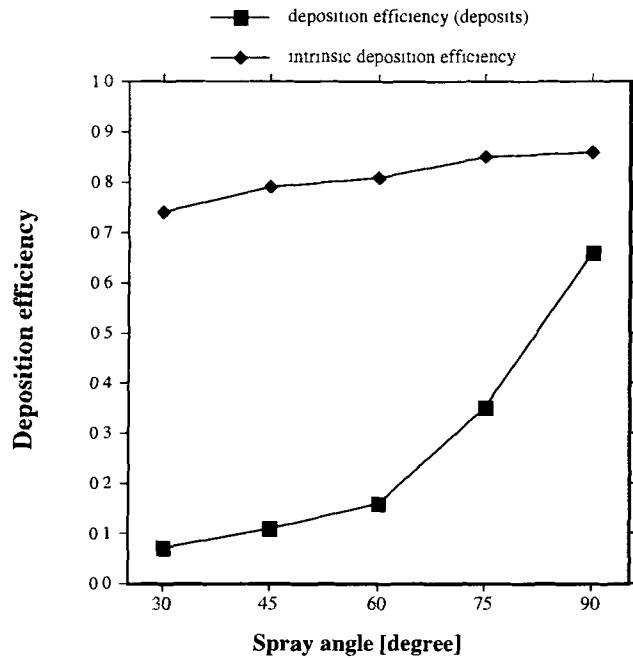
Finally, the high surface roughness ($R_a$) of the thick deposit (3 μm average value versus 0.2 μm average value for the wipe test) can disturb the particle spreading mechanisms, as demonstrated by Smith et al. (Ref 22). In spite of previous limitations, this method can be easily implemented for optimization. It can be used to define size specifications for the powder and to optimize particle size distribution to minimize the loss of powder.

One assumption of the model is a constant thickness of the splats along a random cross section. This is not true for particles impacting with an off-normal spray angle because the particle profiles are wedge-shaped in the impact direction (Ref 11). The lower the spray angle, the more wedge-like the splat thickness profile becomes (wedge angle from 0° for a 90° spray angle to 10° for a 30° spray angle). Moreover, the wedge angle of the selected splats exhibits a near perfect linear dependence on the spray angle. The effect of the spray angle on the secondary particle size distribution is displayed in Fig. 16. The lower the spray angle, the smaller the particle size distribution, leading to the formation of splats. Figure 17 details the lower and upper values



Fig. 19 Comparison of deposition efficiency measured on thick deposits, with the intrinsic deposition efficiency measured on splats, for several spray angles (90° to 30°)
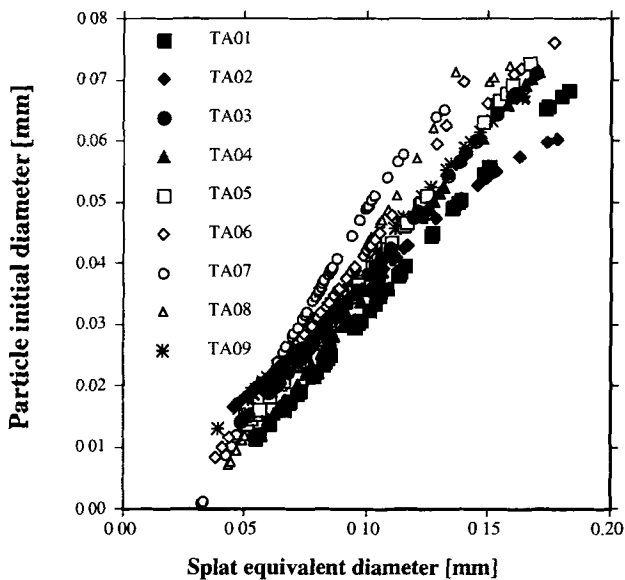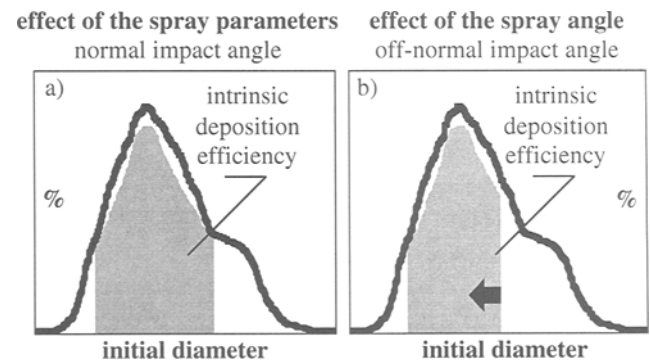


Fig. 20 Effects of (a) the spray parameters and (b) the spray angle on the fraction of the powder particle size distribution leading to the formation of a deposit



Fig. 21 Dependence of the initial powder particle diameter (d) on splat equivalent diameter (ED) for Taguchi spray parameter sets TA01 to TA09
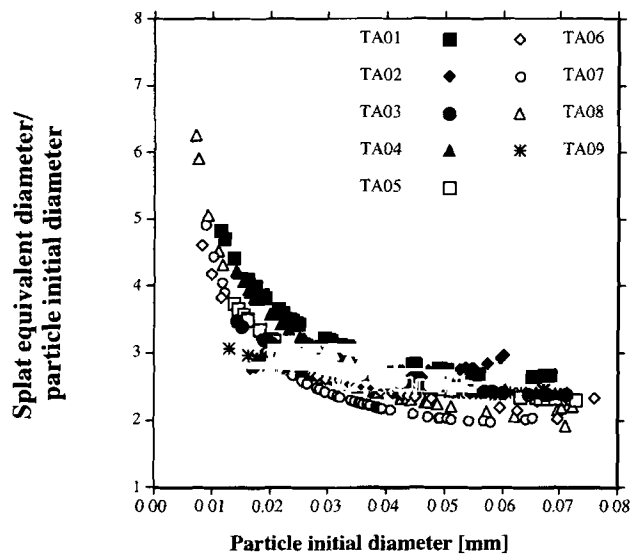


Fig. 22 Dependence of the ratio (ED/d) of the splat equivalent diameter to the initial powder particle diameter on the initial powder particle diameter (d) for Taguchi spray parameter sets TA01 to TA09

of the secondary particle size distributions for each spray angle, while the diameter of the smallest powder particles (particles smaller than 15 μm average diameter), which do not splat, is independent of the spray angle. The diameter of the largest powder particles is significantly affected by the spray angle. To a first approximation, this latter value remains constant when the angle changes from 90° to 60° and then dramatically decreases when the angle changes to 30°.

The lower the spray angle, the less important is the kinetic energy available for spreading the particle, due to decrease of normal velocity, as illustrated in Fig. 18. Meanwhile, the tangential component of the velocity will induce deformation of the splat in the direction of the angle, which will interfere with the spreading mechanism. This effect was not accounted for in the present work and emphasizes the concept of critical impact velocity. Results for intrinsic deposition efficiencies (both calculated and measured deposition efficiencies) are presented in Fig. 19. From a general point of view, the intrinsic deposition efficiency decreases at a lower spray angle, as indicated by Smith et al. (Ref 22). The quantitative differences between the calculated and the measured deposition efficiencies arise for the same reasons previously mentioned for the spray parameter sets, that is, evolution of substrate nature, effects of substrate temperature, and effects of surface roughness, etc.

Figure 20 illustrates the effects of both the spray parameters and the spray angle on the deposited fraction of the powder particle size distribution.

### 4.3 Other Potential Applications of the Model

#### 4.3.1 Powder Particle Initial Diameter

Figure 21 displays dependence of the initial powder particle diameter, calculated using transfer functions for each spray parameter set, on the splat equivalent diameter for Taguchi sets TA01 to TA09. Clearly, an increase in the initial diameter leads to an increase in the resulting equivalent diameter. In a first approximation, these results are equivalent to those obtained by Liu et al. (Ref 23), relative to the two-dimensional Eulerian numerical modeling of the spreading of pure nickel particles on a smooth surface. However, as illustrated in Fig. 22, the dependence of the ratio of the splat equivalent diameter to the initial powder particle diameter (ED/$d$ ratio) on the initial powder particle diameter varies from two (for the smallest impinging particles) to seven (for the largest impinging particles). For all the spray parameters considered, this dependence is the same, except for the TA02 set. This parameter set gives a quasi-constant ratio of approximately three. A homogeneous field of impinging particle velocities could lead to such behavior, which remains to be explained. The smallest powder particles spread more than the largest particles. This signifies that their impact velocity is significantly higher, and that the effect of their impact velocity is greater than the effect of their mass, while the global kinetic energy remains higher for the largest particles, as the results of Fauchais et al. (Ref 19), presented in Fig. 23, suggest.

#### 4.3.2 Impinging Particle Impact Velocity

The impact velocities of the impinging particles that led to the formation of the observed splats were determined using Eq

10. For example, Fig. 24 illustrates the dependence of the impact velocities of the particles (as a function of the splat equivalent diameter) on the ratio of the splat equivalent diameter to the initial powder particle diameter (ED/$d$ ratio), for spray parameter sets TA01 to TA09, following Yoshida's relationship. By curve-fitting, these evolutions can be described by a generic relationship, as follows:

$$V = a \ 10^{ED/d} \tag{Eq 12}$$

where $a$ is a constant equal to $\sim 5 \times 10^{-3}$. These results can be correlated to previously published results (Ref 24 and 25); the effect of the impact velocity on the powder particle has the greatest influence on the shape (equivalent diameter, flattening degree, etc.) of the resulting splat, and the smaller particles impact with higher velocities than the larger particles. Although the impact velocities calculated using Yoshida's relationship are higher than the velocities determined using Trapaga's or Madejski's relationships (for a constant ratio of the splat equivalent diameter to the powder particle equivalent diameter; ED/$d$ ratio) the impact velocities calculated with the model are low compared to those commonly measured (Ref 24) or calculated (Ref 25). In fact, impact velocities as low at 10 m · s$^{-1}$ are obtained, which are unlikely in the case of VPS deposition, as shown in Fig. 25 (Ref 26). This underestimation can arise from (a) the approximations in the calculation of the impact velocity; (b) the use of the kinetic viscosity of pure nickel at melting temperature (viscosity could be significantly different from Astroloy); (c) the assumption that the viscosity is constant, regardless of the particle initial diameter and regardless of temperature of the impinging particles; and (d) the use of Yoshida's relationship, which may not accurately describe the behavior of Astroloy particles impacting on a copper substrate under low residual pressure of an inert gas. The coefficient in this relationship would have to be corrected and adapted. For example, the calculation of an impact velocity of 250 m · s$^{-1}$ for an impinging particle of 30 μm average diameter would use a coefficient close to 0 · 1.



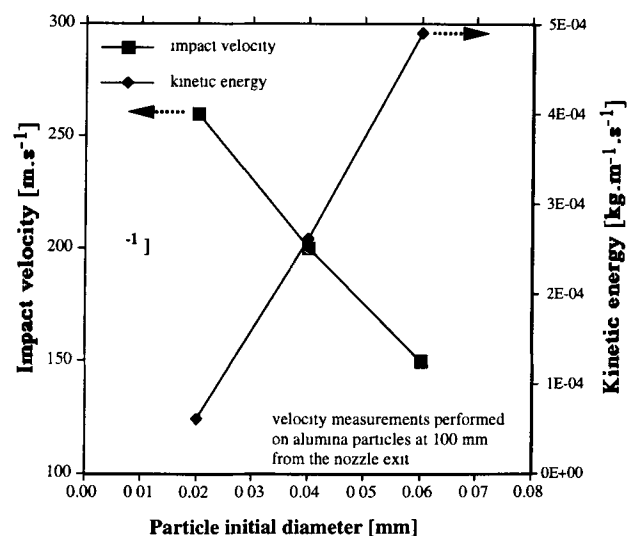Fig. 23 Particle velocity and particle kinetic energy versus distance along the centerline axis of the gun for several particle diameters (Ref 19)
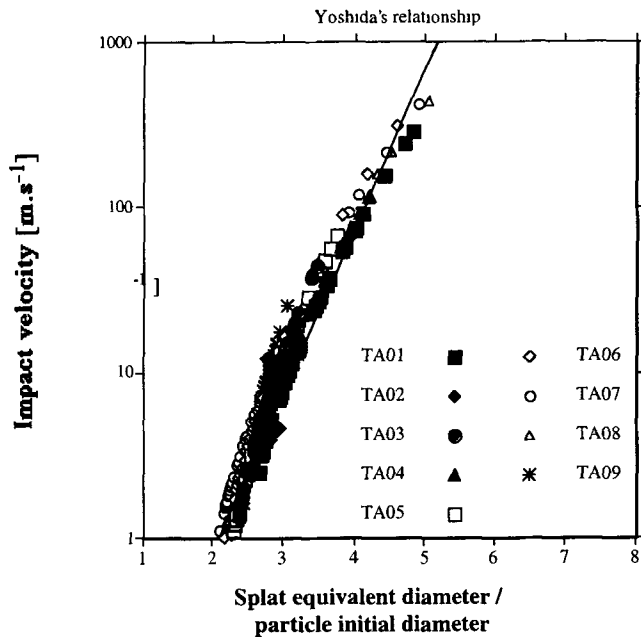
**Fig. 24** Particle impact velocity versus the ratio (ED/d) of initial powder particle diameter for Taguchi spray parameter sets TA01 to TA09, determined by Yoshida's relationship
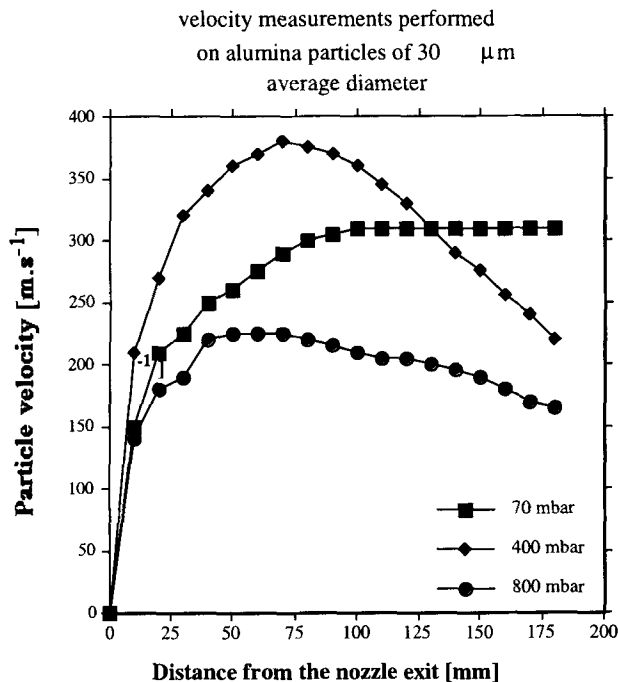


**Fig. 25** Particle velocity as a function of the distance along the centerline axis of the gun for several chamber pressures (Ref 26)

### 4.3.3 Impinging Particle Weber Number

The dimensionless Weber number establishes a relationship between the surface tension and the viscosity of a liquid; the lower the Weber number, the lower the effects of surface tension compared to those of kinetic energy. This number was calculated for each powder particle that became an observed splat, us-

ing Eq 11 and for an impact velocity calculated using Yoshida's relationship. Figure 26 displays the dependence of the dimensionless Weber number on the ratio of the splat equivalent diameter to the initial powder particle diameter (ED/d ratio) for spray parameter sets TA01 to TA09. By curve-fitting, this function is described as follows:

$$We = a \ 10^{b \ ED/d} \qquad \text{(Eq 13)}$$

where $a$ is equal to $-2 \times 10^{-5}$, and $b$ is approximately equal to unity. It appears that the lower ED/d ratio (the higher the powder particle initial diameter), the lower is the corresponding Weber number and the less significant are the effects of surface tension on the particle spreading/flattening compared to the effects of kinetic viscosity. Splashing of particles is linked, in part, with the surface tension and the kinetic viscosity. McPherson predicted splashing particles when the Weber number is greater than 80 (Ref 27). This specific limit does not seem to be applicable to the tests performed in this work; the analyzed splats always showed some splashing. Nevertheless, the same tendency is observed; thus, the particles characterized by low Weber numbers tend to exhibit lower degrees of splashing, as illustrated in Fig. 27.

## 5. Conclusions

In thermal spraying, spreading the impinging particles onto a substrate is a fundamental process in deposit formation. Physical properties and mechanical characteristics of a thermal spray deposit primarily depend on this crucial stage. A simple heuristic model, based on the determination of transfer functions, was developed to investigate the origin of the deposit formation process. The study has demonstrated that it is possible to estimate, a posteriori, the initial diameter of the impinging powder particles that led to the formation of the collected splats, using a few assumptions and knowing the initial powder particle size distribution. This constitutes the basis of a heuristic model, based on the determination of transfer functions, permitting approximation of several characteristic values of the impinging particles, such as the flattening degree, the impact velocity, etc. Among other characteristics, intrinsic deposition efficiency was calculated. This efficiency is the maximum that can be obtained for a given particle size distribution and for given processing parameters (spray parameters, spray angle, etc.). Implementation of this approach has technological and economical impacts; it permits quality control (QC) of the deposition efficiency by control of splat morphology and the optimization of specifications for the powders used, in terms of the lower and upper limits of the particle size distribution leading to the formation of the deposit with given processing parameters. Spray parameters can be optimized to obtain high-integrity deposits.
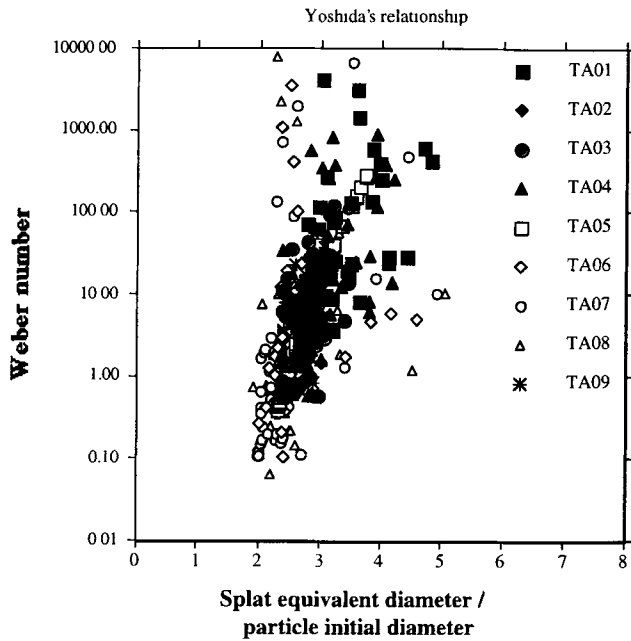
### Acknowledgments

**Fig. 26** Particle dimensionless Weber number as a function of the ratio (ED/*T*) of splat equivalent diameter to initial powder particle diameter for Taguchi spray parameter sets TA01 to TA09, determined by Yoshida's relationship
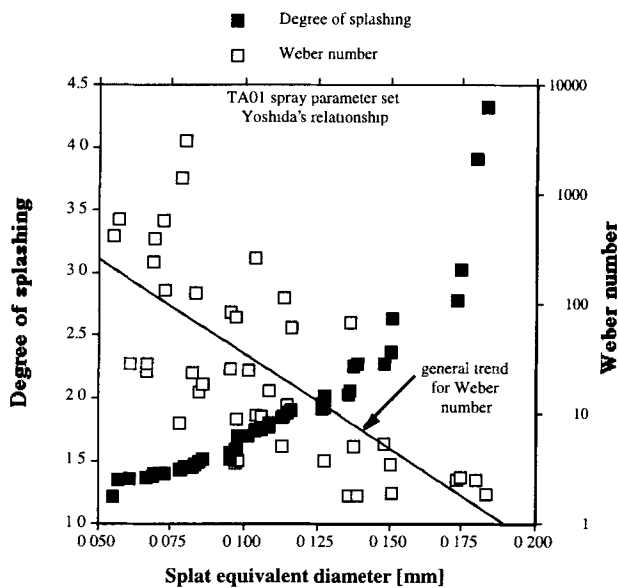


**Fig. 27** Relationship between the splat degree of splashing (DS) and the splat dimensionless Weber number (*We*) as a function of the ratio (ED/*d*) of splat equivalent diameter to initial powder particle diameter for the TA01 Taguchi spray parameter set

## References

1. G. Chadwick, *A System View of Planning*, Pergamon Press, 1971, p 390

2. G. Montavon, S. Sampath, C.C. Berndt, H. Herman, and C. Coddet, Effects of Vacuum Plasma Spray Processing Parameters on Splat Morphology, *J. Therm. Spray Technol.*, Vol 1 (No. 4), 1995, p 67-74

3. G. Montavon, S. Sampath, C.C Berndt, H. Herman, and C. Coddet, Vacuum Plasma Spray Forming of Astroloy: An Investigation of Processing Parameters, *Thermal Spray Industrial Application*, C.C. Berndt and S. Sampath, Ed., ASM International, 1994, p 469-475

4. C.L. Curtis, D.T Gawne, and M. Priestnall, The Electrical Conductivity of Plasma Sprayed Yttria Stabilized Zirconia, *Thermal Spray Coatings: Research, Design and Application*, C.C. Berndt and T.F. Bernecki, Ed, ASM International, 1993, p 519-523

5. L. Bianchi, F. Blein, P. Lucchese, M. Vardelle, A. Vardelle, and P. Fauchais, Effect of Particle Velocity and Substrate Temperature on Alumina and Zirconia Splat Formation, *Thermal Spray Industrial Application*, C C. Berndt and S. Sampath, Ed., ASM International, 1994, p 569-574

6 H.D. Steffens, J Drozak, and D. Haumann, "Morphologie von Spritzteilchen bei verschiedenen Spritzverfahren am Beispiel von Molybdän" (Morphology of Thermal Sprayed Particles in Different Spraying Processes Illustrated by the Behavior of Molybdenum), Deutscher Verlag für Schweißtechnick DVS-Verlag GmbH, Düsseldorf, Germany, 1993, p 366-370, (in German)

7. *Reference Manual*, Tridim, Akilog, Besançon, France, 1994, p 25

8. T.M. Mayhew and L.M. Cruz Orive, Caveat on the Use of the Delesse Principle of Aeral Analysis for Estimating Component Volume Densities, *J. Microsc.*, Vol 102 (No. 2), 1974, p 195-207

9. NIH Image 1.59 Reference Manual, National Institutes of Health, 1994

10. J.C. Russ, *The Image Processing Handbook*, 2nd ed., CRC Press Inc., 1995, p 674

11. G. Montavon and C. Coddet, 3-D Profilometries of Vacuum Plasma Sprayed Nickel-Based Alloy Splats Using Scanning Mechanical Microscopy, *Thermal Spray Science and Technology*, C.C. Berndt and S. Sampath, Ed., ASM International, 1995, p 285-289

12. S. Fantassi, M. Vardelle, A. Vardelle, and P. Fauchais, Influence of the Velocity of Plasma Sprayed Particles on the Splat Formation, *Thermal Spray Coatings: Research, Design and Applications*, C.C. Berndt and T.F Bernecki, Ed., ASM International, 1993, p 1-6

13 G. Trapaga and J. Szekely, Mathematical Modeling in the Isothermal Impingement of Liquid Droplets in Thermal Spraying, *Metall. Trans. B*, Vol 22, 1991, p 901-914

14. J. Madejski, Solidification of Droplets on a Cold Surface, *Int. J. Heat Mass Transfer*, Vol 19, 1976, p 9-20

15. I. Egry, On the Relation Between Surface Tension and Viscosity for Liquid Metals, *Scr. Metall. Mater.*, Vol 28, 1993, p 1273-1276

16. J.K. Vennard and R.L. Street, *Elementary Fluid Mechanics*, 5th ed., John Wiley and Sons Inc., 1976, p 740

17. X. Chen and E. Pfender, Behavior of Small Particles in a Thermal Plasma Flow, *Plasma Chem. Plasma Process.*, Vol 3 (No. 3), 1983, p 351-356

18. X. Chen and E. Pfender, Effect of the Knudsen Effect on the Heat Transfer to a Particle Immersed into a Thermal Plasma, *Plasma Chem. Plasma Process.*, Vol 3 (No. 2), 1983, p 97-114

19. P. Fauchais, A. Vardelle, M. Vardelle, J.F. Coudert, and J. Lesinski, Correlation of the Physical Properties of Sprayed Ceramic Coatings to the Temperature and Velocity of the Particles Travelling in Atmospheric Plasma Jets. Measurements, Travelling and Comparison, *Thin Solid Films*, (No. 121), 1984, p 303-316

20. M. Fukumoto, S. Katoh, and I. Okane, Splat Behavior of Plasma Sprayed Particles on Flat Substrate Surface, *Thermal Spraying: Current Status and Future Trends*, A. Ohmori, Ed., High Temperature Society of Japan, Osaka, Japan, 1995, p 353-358

21. L. Bianchi, P. Lucchese, A. Denoirjean, and P. Fauchais, Zirconia Splat Formation and Resulting Coating Properties, *Thermal Spray Science and Technology*, C.C. Berndt and S Sampath, Ed., ASM International, 1995, p 261-266

22. M.F. Smith, R.A. Neiser, and R.C. Dykhuizen, An Investigation of the Effects of Droplet Impact Angle in Thermal Spray Deposition, *Thermal Spray Industrial Application,* C C. Berndt and S. Sampath, Ed., ASM International, 1994, p 603-608

23. H. Liu, E. Mühlberger, A Sickinger, E.J. Lavernia, and R.H. Rangel, Numerical Investigation of Micro-Pore Formation During Substrate Impact of Molten Droplets in Spraying Processes, *Thermal Spray Industrial Application,* C.C. Berndt and S. Sampath, Ed., ASM International, 1994, p 375-380

24. C. Moreau, P. Gougeon, M. Lamontagne, V. Lacasse, G. Vaudreuil, and P. Cielo, On-Line Control of the Plasma Spraying Process by Monitoring the Temperature, Velocity, and Trajectory of In-Flight Particles, *Thermal Spray Industrial Application,* C C Berndt and S Sampath, Ed., ASM International, 1994, p 431-437

25. H. Liu, E.J. Lavernia, and R.H. Rangel, Numerical Simulation of the Impingement of Molten Ti, Ni, and W Droplets on a Flat Substrate, *J. Therm. Spray Technol.,* Vol 4 (No. 2), 1993, p 369-378

26. M F. Smith and R.C. Dykhuizen, Effect of Chamber Pressure on Velocities in Low Pressure Plasma Spray Deposition, *Surf. Coat. Technol.,* (No. 34), 1988, p 25-31

27. W.R. McPherson, The Relationship Between the Mechanism of Formation, Microstructure and Properties of Plasma-Sprayed Coatings, *Thin Solid Films,* (No 83), 1981, p 297-310